JACS
JOURNAL OF THE AMERICAN CHEMICAL SOCIETY

ARTICLE

pubs.acs.org/JACS

Metal Ion Affinity-based Biomolecular Recognition and Conjugation inside Synthetic Polymer Nanopores Modified with Iron−Terpyridine Complexes

Mubarak Ali,*[,†,‡] Saima Nasir,[†,‡] Quoc Hung Nguyen,[†,‡] Jugal Kishore Sahoo,[§] Muhammad Nawaz Tahir,[§] Wolfgang Tremel,[§] and Wolfgang Ensinger[†,‡]

[†]Technische Universität Darmstadt, Department of Material- and Geo-Sciences, Petersenstrasse 23, D-64287 Darmstadt, Germany
[‡]Materials Research Department, GSI Helmholtzzentrum für Schwerionenforschung, Planckstrasse 1, D-64291 Darmstadt, Germany
[§]Department of Chemistry, Johannes Gutenberg-Universität, Duesbergweg 10-14, 55099 Mainz, Germany

Supporting Information

ABSTRACT: Here we demonstrate a novel biosensing platform for the detection of lactoferrin (LFN) via metal−organic frameworks, in which the metal ions have accessible free coordination sites for binding, inside the single conical nanopores fabricated in polymeric membrane. First, monolayer of amine-terminated terpyridine (metal−chelating ligand) is covalently immobilized on the inner walls of the nanopore via carbodiimide coupling chemistry. Second, iron−terpyridine (iron−terPy) complexes are obtained by treating the terpyridine modified-nanopores with ferrous sulfate solution. The immobilized iron−terPy complexes can be used as recognition elements to fabricate biosensing nanodevice. The working principle of the proposed biosensor is based on specific noncovalent interactions between LFN and chelated metal ions in the immobilized terpyridine monolayer, leading to the selective detection of analyte protein. In addition, control experiments proved that the designed biosensor exhibits excellent biospecificity and nonfouling properties. Furthermore, complementary experiments are conducted with multipore membranes containing an array of cylindrical nanopores. We demonstrate that in the presence of LFN in the feed solution, permeation of methyl viologen (MV^{2+}) and 1,5-naphthalenedisulphate (NDS^{2-}) is drastically suppressed across the iron−terPy modified membranes. On the basis of these findings, we envision that apart from conventional ligand−receptor interactions, the designing and immobilization of alternative functional ligands inside the synthetic nanopores would extend this method for the construction of new metal ion affinity-based biomimetic systems for the specific binding and recognition of other biomolecules.

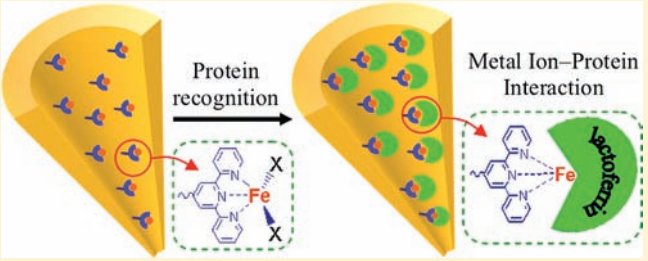

1. INTRODUCTION

During the recent years, solid-state nanopores have gained considerable attention of scientific community because of their unique ionic transport properties, providing an excellent platform for potential applications, such as biosensing,[1−8] molecular separation,[9−13] and targeted drug delivery[14−16] at the nanoscale level. Biological ion channels in living organisms facilitate the diffusion of ions, water, or small organic molecules across the cell membrane, portray a perfect example from nature.[17] However, because of fragility and sensitivity of the embedding lipid bilayer, biological pores are not suitable for practical applications. On the contrary, synthetic nanopores display several advantages over their biological counterparts, especially: stability, control over pore shape and diameter, possibility of integration into nanofluidic devices, and modifiable surface properties for interaction with molecules of interest.[18−22]

To date, different strategies have been developed for the fabrication of nanoscale architectures to maintain a natural environment in an artificial device that closely mimic biological system.[18−20,22] Compared with other techniques, ion-track-technology[23,24] offers a unique possibility to fabricate single pore, as well as multipore, membranes, depending on the number of heavy ions penetrated. Second, it also provides flexibility to control both pore shape (e.g., conical, cylindrical, or biconical) and size, down to a few nanometers. Track-etched nanopores also display transport properties similar to that of biological ion channels, such as ion current rectification, voltage-dependent current gating, and selective ion permeation.[25−30] The chemical functionalities on the pore surface are crucial for the above-mentioned applications, since they strongly influence the ionic transport through the nanopore.[31−33] The immobilized ligands onto the surface and inner walls of the nanopores would serve as binding or sensing sites for different analytes as well as interact with molecules passing through the pore.[2,3,8,34−38]

Received: June 1, 2011
Published: September 19, 2011

dx.doi.org/10.1021/ja205042t | J. Am. Chem. Soc. 2011, 133, 17307–17314

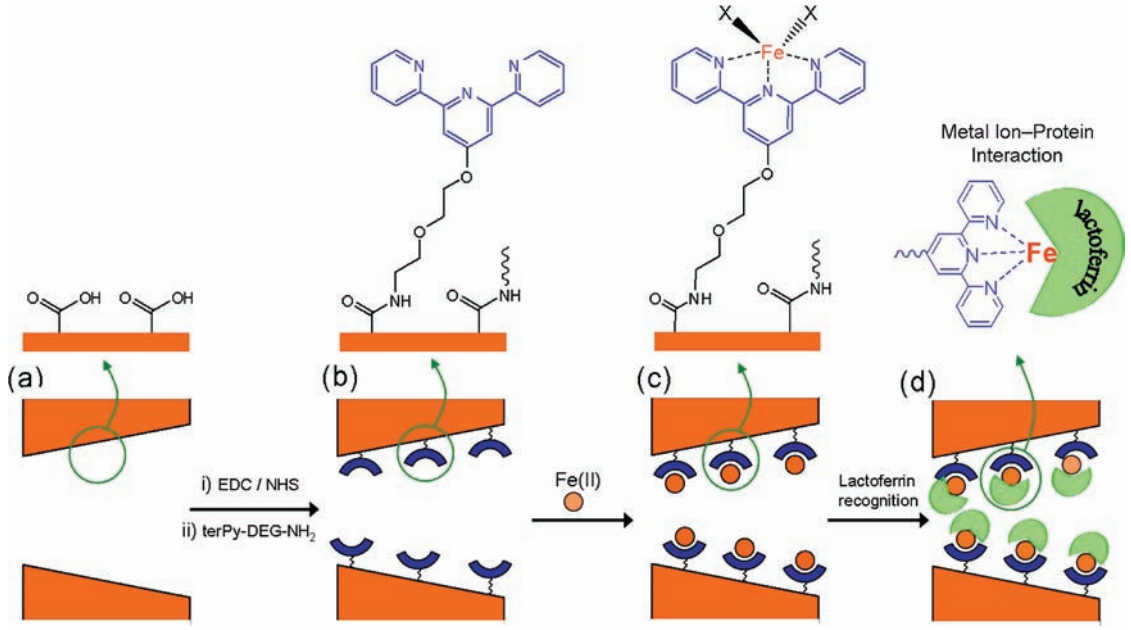

Figure 1. Schematic representation of (a) as-prepared single conical nanopore containing surface carboxylic acid groups, (b) covalent immobilization of amine-terminated terpyridine ligand with carboxyl groups via carbodiimide coupling chemistry, (c) subsequent treatment with iron(II) salt solution to obtain iron−terPy complexes (X represents any counterion or coordinating solvent molecule), and (d) biorecognition of lactoferrin molecules.

The immobilization of biorecognizable elements into these nanoscale architectures have been achieved mainly through covalent attachment, and electrostatic self-assembly of functional polyelectrolytes onto the interior of the nanopore by exploiting the existing chemical groups on the pore surface. Seminal work of Martin et al. demonstrated the covalent immobilization of thiol-terminated organic/biomolecules on the inner wall of gold-coated nanopores inside polymeric membrane for protein sensing and permselective ionic transport.[9−12,38] More importantly, track-etched nanopores in polyethylene terephthalate (PET) membranes possesses carboxylic acid functionalities on the surface and inner walls.[1,26,39,40] We and others have also reported the direct covalent attachment amino-terminated molecules onto the inner pore surface.[8,33,41−44] Moreover, biomolecular immobilization has also been achieved via electrostatic interactions onto the surface and inner walls of the nanopore.[3,39,45] Recently, we have also demonstrated biomolecular immobilization onto the interior of the nanopore through sugar−lectin biospecific interactions.[46] However, previously developed biosensing nanodevices were mainly based on conventional ligand−receptor interactions, such as protein−protein,[46] biotin−streptavidin/avidin,[3,8,38] antigen−antibody binding,[38,47] and peptide nucleic acid−DNA interactions,[1,48] leading to the blockage of the pore opening or modulation of pore surface charge. To further expand the potentialities of these nanosized systems, decorating of nanopore interior with metal chelating organic ligands would also provide another biosensing platform for the immobilization and detection of biomolecules that display affinity toward specific metal ions.

Among the various organic metal−chelating ligands, terpyridine (terPy) is quite attractive because of its ability to form stable complexes with different metallic ions (Fe, Co, Ni, Zn, etc.).[49] On the basis of the metal ion affinity approach, Tuccitto et al. have already been demonstrated the successful immobilization of lactoferrin (LFN) onto the gold surface via a patterned self-assembled monolayer containing iron−terpyridine complexes.[50,51] Lactoferrin is widely distributed in mammalian physiological secretions, such as milk, saliva, tears, and seminal fluids.[52−54] LFN is also recognized as an iron−binding glycoproteins which play a key role in the transport of iron in biological systems.[55,56] In recent years, LFN is successfully used as a carrier for drugs to target brain tumer.[57,58] Moreover, LFN also play an important role in the host defense system against microbial and viral infections.[59−62] Naturally, LFN molecule possesses two specific iron-binding sites. These binding sites are localized in each of the two homologous globular domains named N-and C-lobes. Each LFN molecule can reversibly bind with two ions of iron. The coordination of iron cation involves four amino acid residues in each lobe: two tyrosine residues, one histidine residue, and one aspartic acid residue.[52,56]

Herein, we present a biosensing platform based on the specific noncovalent interactions between LFN and metallic ion chelated in terPy monolayer, immobilized on the inner walls of track-etched nanopores. For this purpose, the interior of the nanopore is tailored with terpyridine ligand. Subsequently, modified nanopores are treated with a solution of iron(II) salt to form iron−terPy complexes, which acted as recognition elements for the capturing of LFN molecules. The success of chemical reactions and biorecognition events are confirmed *via* ionic current passing through the nanopore by measuring the current−voltage ($I-V$) characteristics of the single-pore membranes. The modified nanopores are successfully used as nanobiosensor for the specific detection of LFN. In addition, complementary experiments are performed by using multipore polymer membranes. In this case, after immobilization of iron−terPy complexes onto the pore surface, permeation of doubly charged organic analyte through a cylindrical nanopore array is suppressed by the coaddition of LFN in the feed solution.

2. RESULTS AND DISCUSSION

Polyethylene terephthalate (PET) membranes containing single conical nanopores and a cylindrical nanopore array

(10^8 pores cm^{-2}) were used in this study. Single conical nanopores were fabricated via asymmetric chemical etching of the latent track of a single energetic heavy ion.[30] On the other hand, multitrack array membranes were etched symmetrically for the fabrication of cylindrical nanopores.[63,64] PET is a polyester, and the etchant (NaOH) species preferentially attack on the partially charged ester groups. As a result of track-etching process, approximately one carboxyl (−COOH) group per nm^2 is exposed on the nanopore surface because of the cleavage of polymeric chains.[65] These groups can act as sites for the covalent attachment of desired ligand molecules on the interior of the nanopore surface.

The metal−chelating ligand used in this study is 1-amino-5-(2,2′:6′,2″-terpyrid-4′-yl-oxy) pentane (terPy-DEG-NH_2). The ligand was synthesized by the direct coupling of diethylene glycolamine (DEG-NH_2) with 4′-chloro,2,2′:6′,2″-terpyridine (terPy) molecule.[66] The primary amine on one terminus of the ligand (terPy-DEG-NH_2) was exploited for the covalent linkage with surface −COOH groups, while terpyridine moiety on the other terminus used for metal ion complexation.

Here, we demonstrated the covalent attachment of surface −COOH groups with terminal amine of the ligand (terPy-DEG-NH_2). To achieve this, carboxyl groups were first activated into amine-reactive sulfo-NHS ester molecules by using an aqueous solution of *N*-(3-dimethylaminopropyl)-*N*′-ethylcarbodiimide HCl (EDC) and *N*-hydroxysulfosuccinimide (sulfo-NHS).[67] Subsequently, the succinimidyl intermediate was covalently coupled with the amine of the ligand via stable amide linkage. After modification, the iron−terpyridine (iron−terPy) complex was achieved by treating the modified pore with an aqueous ethanolic solution of ferrous sulfate (Figure 1).[50,51]

Before modification, pore walls are negatively charged at neutral pH because of the presence of ionized carboxyl ($-COO^-$) groups. Therefore, the nanopore volume in an aqueous solution is mainly filled with ions of charge opposite to that of the fixed charged groups on the pore surface. In the present case, the unipolar solution of positive ions inside the nanopores is responsible for the observed electrical conductance at each potential difference applied externally. It is well-known that single conical nanopores rectify the ionic current due to an asymmetry in the intrinsic electrostatic potential along the pore axis.[27,28,31,68−73]

I−*V* characteristics of single conical nanopores in PET membranes were recorded in symmetric electrolyte conditions on both sides of the membrane using 0.1 M KCl solution as an electrolyte at neutral pH. The direction of rectification in conical channels is solely based on surface charge.[74−76] Before modification, pore rectifies the cation current with the preferential direction of the cation flow from the narrow opening to the wide opening of a cone because of the presence of inherent $-COO^-$ groups (Figure 2). Based on the electrode configuration in our system, higher currents are recorded for positive voltages, while lower value of negative ionic currents is observed due to the cations flow from the wide opening toward the narrow tip of the cone at reversed voltages. After modification, monolayers of iron−terPy complexes switched the surface charge from negative to neutral, resulting in the loss of rectification behavior as exhibited from the current−voltage (*I*−*V*) curve shown in Figure 2. This clearly confirmed the successful anchoring of chelated metal ions onto the inner walls of the nanopore.

The bioconjugation process confined into a nanopore would lead to volume exclusion or electrostatic-based effects, which govern the ionic mass transport across the nanopore. Here, our

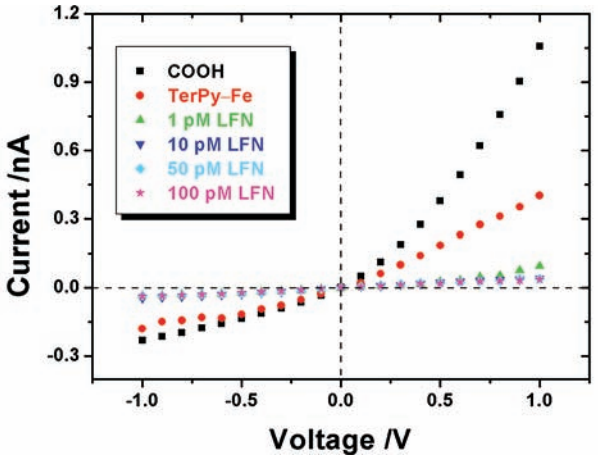

Figure 2. *I*−*V* characteristics of a single conical nanopore with tip $d \approx$ 13 nm measured in 0.1 M KCl (pH 7.0) solution corresponding pore surface with carboxylate groups (black square), and iron−terpyridine complexes (red filled circle); and upon exposing the modified pore to different concentration of lactoferrin prepared (separately) in the same electrolyte solution, respectively.

main concern is with the volume exclusion principle because molecular size of analyte is comparable to the tip opening of the nanopore.[3,38] Thus, the binding of biomolecular analyte to the pore walls would lead to the partial or complete occlusion of the pore opening and would hinder the flow of ions across the membrane. Consequently, the molecular recognition process would promote a sensitive change in the magnitude of the ionic current passing through the nanopore.

Analytical parameters, such as sensitivity and selectivity (specificity), should also be taken into account, when designing a biosensing platform. The sensitivity of the designed biosensor was evaluated by exposing the modified pore to different concentrations of analyte (LFN) protein, prepared in the working electrolyte solution. Figure 2 shows the change in the *I*−*V* characteristics upon exposing the iron chelated nanopore to various concentrated LFN solutions. As expected, the presence of LFN in the background electrolyte, even at very low concentrations, resulted in a drastic decrease in the ion flux across the nanopore. From the *I*−*V* curve, the ionic transport across the modified nanopore was 400 pA at a potential of +1 V. The binding of LFN to chelated iron ion inside the nanopore led to a significant decrease in the effective diameter which in turn impact the ionic flux through the nanopore. Upon exposure to a LFN solution of only 1pM, the observed value of ionic current for +1 V was dropped from 400 to 95 pA. Similarly, the ion current measured at the reverse bias, that is, −1 V, also decreased from 180 to 35 pA. This means that 1 pM solution of LFN promoted a ∼76% and ∼80% decrease in the ion flux through the pore at +1 V and −1 V, respectively. The observed decrease in the ionic current was because of the formation of bioconjugates onto the inner pore surface. With 10 pM LFN solution, ionic current was further decrease to 41 pA at positive potential which correspond to ∼90% reduction in ionic flux, compared to the modified pore without bioconjugation. From the *I*−*V* data shown in Figure 2, it is evident that the modified pore become saturated with bioconjugates with 10 pM LFN solution. Further an increase in LFN concentration did not induce any significant change in the ionic current flowing across the nanopore at both positive and negative voltages. It has already been reported that bioconjugation of

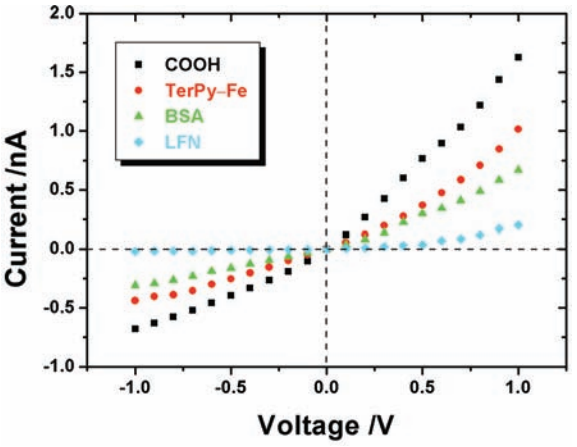

Figure 3. Current−voltage characteristics of a single conical nanopore with tip $d \approx 11$ nm and base $D \approx 575$ nm in 0.1 M KCl prior to and after the covalent immobilization of iron−terPy ligand followed by the addition (separately) of 100 nM of each, bovine serum albumin (BSA) and lactoferrin (LFN) protein in the electrolyte solution, respectively.

protein analytes in conical shaped gold nanotubes and nanopores through ligand−receptor interactions onto the inner walls clogged the tip opening, leading to the permanent blockage of the ion current.[3,38] The above experimental results provide clear evidence that the metal ions in the immobilized ligand (iron−terPy) are able to biorecognize receptors (LFN) even at very low concentrations in the surrounding environment, and this biorecognition can be transduced in an electronic signal originating from the ionic transport thorough the nanopore.

Second, selective (specific) recognition of the target analyte is also a most desirable characteristic of a biosensor, that is, biosensors should also exhibit selectivity for the detection and transduction of specific events upon the binding of analyte molecules. In other words, to demostrate that this approach is valid to create a biosensing platform inside the nanoconfined geometry, it is important to show that the changes in the ionic current are mainly due to the biorecognition events, and not to the mere physical adsorption of protein analyte onto the pore surface. To verify the selectivity/specificity of the iron−terPy-modified nanopore, we repeated the same experiment using bovine serum albumin (BSA) and lactoferrin (LFN) protein analytes, respectively. Figure 3 shows that the presence of BSA in the background electrolyte in contact with modified nanopore could not led to the blockage of the ionic flux across the nanopore. This confirmed the lack of binding capability of BSA toward chelated metal ion, leaving the original surface remain undisturbed with free coordination sites of metal cations in the iron−terPy monolayers. Subsequently, when the same pore was exposed to lactoferrin (LFN) protein, bioconjugation occurred because of the specific metal ion−protein binding interactions, leading to a decrease of ∼80% at +1 V and ∼95% at reversed voltage bias (−1 V) in the ionic current, compared to the modified pore without bioconjugation (Figure 3). From the $I-V$ characteristics, we can infer that the presented sensor exhibits a remarkable selectivity and specificity toward LFN because of natural possession of iron−binding sites in the globular domain of that protein.

Additionally, a negative control experiment was also performed in the same set of experimental conditions with unmodified (carboxylated) and terPy-modified (Figure 1b) single conical nanopore without iron complexation. It is evident from the $I-V$ characteristics shown in Figure 4 that even working with higher concentration of LFN in the background electrolyte, we did not observe any significant change in the ionic current passing through the as-prepared (carboxylated) and terPy-modified nanopore. These experimental results were further supported our finding that LFN can only specifically bind with chelated metal ion in the terPy-iron complexes immobilized on the inner walls of the pores.

Moreover, to support and confirm the proposed ligand−receptor interaction based on metal ion affinity approach, complementary experiments were conducted using multipore membranes containing an array of cylindrical nanopores with an areal density of 10^8 pores cm^{-2}. The influence of lactoferrin on the selective permeability was investigated by monitoring the ionic permeation of doubly charged organic analytes across the nanoporous membrane. The membrane was clamped between the two halves of the conductivity cells. The feed half-cell contained a known concentration of methylviologen (MV^{2+}) or 1,5-naphthalenedisulfonate (NDS^{2-}) analyte (separately). The permeate half-cell was filled with pure buffer solution. At fixed periods of time, the concentration of analyte in the permeate half-cell was obtained by measuring the UV absorbance with a UV/vis spectrometer.

Figure 5 shows the permeation data versus time of charged analytes (MV^{2+} and NDS^{2-}) across the nanoporous membrane before modification and after iron−terpy immobilization followed by the bioconjugation onto the pore surface. The diffusion data reveals the number of moles of the charged molecules transported per cm^2 area of the membrane. Both MV^{2+} and NDS^{2-} molecules have quite similar molecular volumes of 0.637 and 0.680 nm^3, respectively.[77] Furthermore, the molecular structures of both MV^{2+} and NDS^{2-} analytes contain two benzyl rings, which determine their same hydrophobic behavior within the nanopores.[63] Therefore, the volume exclusion and hydrophobic interaction mechanisms can be neglected in the case of as-prepared (unmodified) multipore membranes. Hence, in our system, the electrostatic interaction between charged analytes (MV^{2+} and NDS^{2-}) in solution and fixed negative ($-COO^-$) charges on the inner walls of the pore was the main driving force, responsible for the permeation variation across the membrane (Figure 5a). Initially, an electrical double layer was generated inside the nanopore which contains a higher concentration of MV^{2+} cations, compared to NDS^{2-} analyte anions. Therefore, MV^{2+} ions selectively diffused across the membrane, while co-ions (NDS^{2-}) are electrostatically prohibited from entering the nanopore. Therefore, diffusion of MV^{2+} is much higher than that of the NDS^{2-} molecules in the permeate compartment (Figure 5a).[63]

Figure 5b showed that after the immobilization of iron−terPy complexes onto the pore surface, the diffusion of MV^{2+} molecules was also drastically decreased in the presence of LFN in the feed solution. A plausible explanation for the observed decrease in permeation is that the LFN bioconjugates inside the pore significantly reduced the effective pore diameter available for the ionic transport. This in turn suppressed/hindered the flow of analyte molecules across the membrane. Therefore, selective permeation of analyte was lost after LFN conjugation, and now the volume exclusion principle mainly governs the ionic transport across the membrane. The permeation data shown in Figure 5b indicated that the permeation of MV^{2+} ions was almost

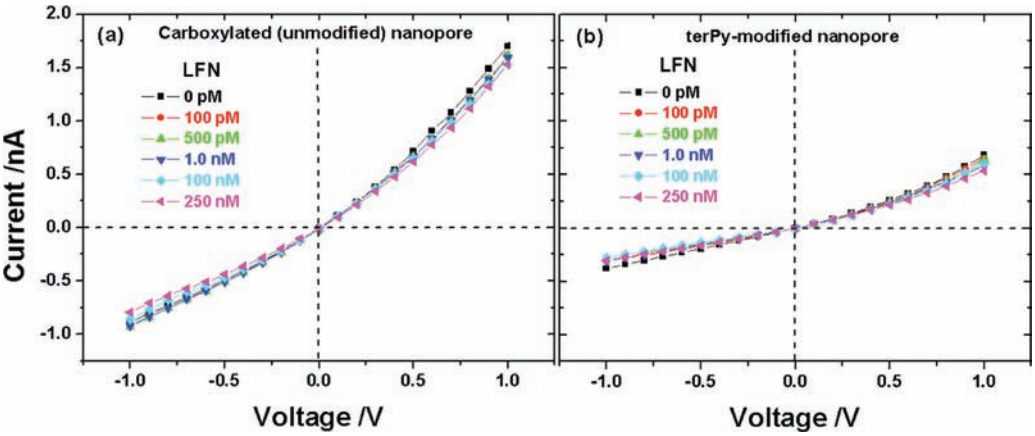

Figure 4. Current−voltage ($I-V$) characteristics of a single conical nanopore with tip $d \approx 10$ nm in 0.1 M KCl solution (a) before and (b) after the covalent attachment of terpyridine, followed by the addition of various concentration of lactoferrin in the background electrolyte solution.

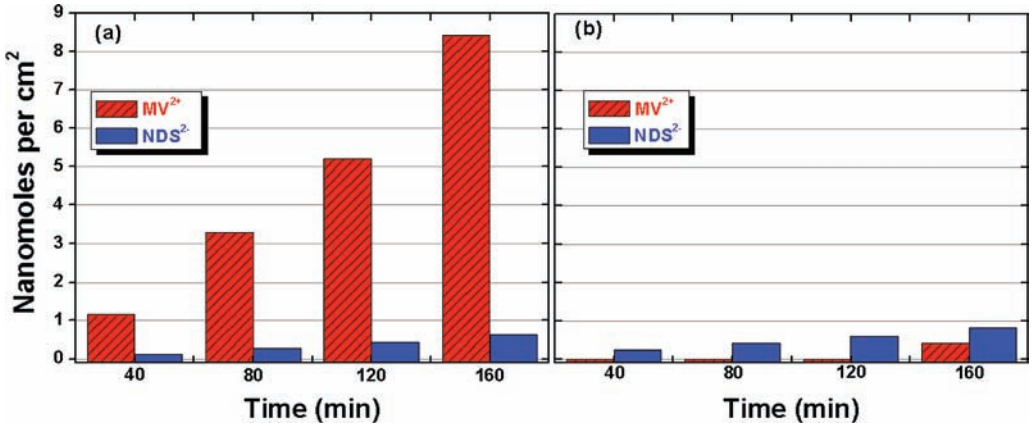

Figure 5. Diffusion of doubly charged organic analytes (MV^{2+} and NDS^{2-}) through nanoporous membrane containing an array of cylindrical nanopores (10^8 pores cm^{-2}) of ~18 nm in diameter, (a) before modification (carboxylated pore surface) without lactoferrin in the feed solution, and (b) after the immobilization of iron−terPy complexes in the presence of lactoferrin (100 nM) in the feed solution.

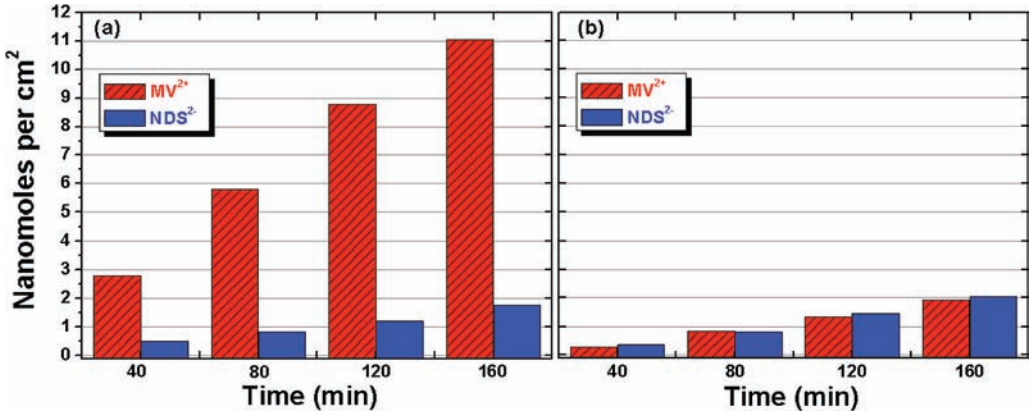

Figure 6. Diffusion of doubly charged organic analytes (MV^{2+} and NDS^{2-}) in the presence of lactoferrin (100 nM) in the analyte solution through nanoporous membrane containing an array of cylindrical nanopores (10^8 pores cm^{-2}) of ~26 nm in diameter, (a) before modification (carboxylated pore surface), and (b) after the immobilization of iron−terPy complexes onto the inner walls of nanopores.

blocked, i.e., no detectable amount of these ions was transported across the membrane until 120 min of diffusion time. However, the permeation of MV^{2+} ions after 160 min was only 0.42 nanomoles which is negligible when compared with 8.4 nanomoles corresponding to as-prepared (unmodified) membrane.

However, question may arise that this decrease in ionic permeation is either due to the formation of bioconjugates or only because of the physical adsorption of LFN molecules onto the nanopore surface. To assure this, we carried out the same diffusion experiment with another multipore membrane under the same set of experimental conditions. Figure 6 describes the ionic (MV^{2+} and NDS^{2-}) permeation versus time across the membrane before and after the iron−terPy immobilization in the presence of LFN dissolved in the feed solution. The diffusion data shown in Figure 6a reveals that the presence of LFN molecules did not cause any interference in the selective diffusion of MV^{2+} ions across the negatively charged ($-COO^-$) multipore membrane. However, when the same membrane was modified with metal−chelates, selective permeation of MV^{2+} was drastically reduced from 11.0 to 1.9 nanomoles after 160 min of diffusion time (Figure 6b). The above-mentioned experimental results showed that the chelated metal ions affinity based LFN bioconjugation indeed diminishes the effective pore diameter available for the transport of analyte molecules. This resulted in a decrease of ∼82% in the permeation of MV^{2+} across the modified membrane. These results provided clear evidence that metal ions incorporated in the immobilized terPy monolayers onto the nanopore surface are accessible to analyte protein for successful binding through specific noncovalent interactions inside the confined environment.

3. CONCLUSIONS

In summary, we experimentally demonstrated the construction of a nanobiosensor based on the immobilization of metal−ligand complexes inside confined environment for the selective biomolecular recognition through metal−protein specific interactions. To achieve this goal, terpyridine ligands were covalently attached inside the track-etched nanopores by exploiting inherent COOH groups via EDC/sulfo-NHS coupling chemistry, followed by the iron complexation. The experimental results showed that the immobilized ligand (iron−terPy complex) were acted as biorecognition element for the specific detection of LFN molecules. In addition, control experiments proved that the designed biosensor exhibit excellent biospecificity and nonfouling properties. For the further confirmation of noncovalent interaction of lactoferrin with iron complex, complementary experiments were also performed with multipore polymer membranes. We demonstrated that in the presence of LFN in the feed solution, permeation of methyl viologen (MV^{2+}) and 1,5-naphthalenedisulphate (NDS^{2-}) is drastically suppressed across the iron−terPy modified membranes, representing the occlusion of the nanopore upon the binding of LFN with metal ions incorporated into metal−chelating ligand. In this context, we believe that metal affinity-based biomimetic system can be further extended for the molecular recognition of other protein analytes possessing specific receptors for coordination with metal ions in their polypeptide backbone. For instance, chelated nickle (Ni^{2+}) ions preferably bind to histidine rich proteins, or those protein containing an exposed histidine tail (His-tagged proteins). Similarly, proteins containing zinc finger motifs (zinc finger proteins) can specifically coordinate and binds with zinc (Zn^{2+}) ions chelated with a ligand.

4. MATERIALS AND METHODS

4.1. Materials. All the reagents used were of analytical grade and used as received without further purification. Methylviologen dichloride (MV^{2+}), 1,5-naphthalene disulfonate disodium salt (NDS^{2-}), *N*-(3-dimethylaminopropyl)-*N*′-ethylcarbodiimide hydrochloride (EDC), *N*-hydroxysulfosuccinimide (sulfo-NHS), 2-(2-aminoethoxyethanol) (AEE), bovine serum albumin (BSA; fraction V), lactoferrin human (LFN), ferrous sulfate heptahydrate ($FeSO_4 \cdot 7H2O$), dimethyl sulfoxide (anhydrous, DMSO), and 4′-chloro,2,2′,6′,2″-terpyridine were purchased from Sigma-Aldrich, Germany. 2-(*N*-Morpholino)ethanesulfonic acid (anhydrous, MES) was purchased from SL Labor-Service GmbH, Germany.

Polymer foils of polyethylene terephthalate (PET) of 12 μm thickness (Hostaphan RN 12, Hoechst) were irradiated at the linear accelerator UNILAC (GSI, Darmstadt) with single, as well as 10^8 swift heavy ions (Pb, U or Au) per cm^2 having an energy of 11.4 MeV per nucleon.

4.2. Fabrication of Nanopores. Before the track-etching process, heavy ion tracked membranes were sensitized with UV light (UV source provided a light intensity of 30 W m^{-2}, with the maximum wavelength at 320 nm) for 15 min on each side to improve the etching properties of latent tracks inside the polymer membrane.

4.2.1. Preparation of Single Conical Nanopores. The fabrication of single conical nanopores in PET membranes was achieved by an asymmetric track-etching technique developed by Apel and coworkers.[30] Briefly, the heavy ion-irradiated membrane was placed between the two halves of a conductivity cell in which the membrane served as a dividing wall between the two compartments. An etching solution (9 M NaOH) was added on one side, while the other side of the cell was filled with stopping solution (1 M HCOOH + 1 M KCl). The stopping solution protected one side of the membrane from etching, and assured the conical geometry of the resulting nanopores. Etching process was carried out at room temperature, and a potential of −1 V was applied across the membrane during the whole process to monitor the ion current passing through the nascent pore. The current remained zero as long as the pore was not yet etched through. After the breakthrough, the stopping solution on the other side of the membranes neutralized the etchant. The etching process was stopped when the current reached a value of ∼0.1 nA. Then the pore was washed first with stopping solution to quench the etchant, followed by rinsing with deionized water. The etched membrane was immersed in deionized water overnight to remove the residual salts.

After etching, large opening diameter of the conical pore was determined by field emission scanning electron microscopy (FESEM). For this purpose a PET sample containing 10^7 ions cm^{-2} was etched simultaneously with the single ion tracked membrane under the same conditions. The diameter of the small opening is below the FESEM resolution and was determined from the current−voltage ($I-V$) curves by using the following relation

$$d = 4LI/\pi D\kappa V$$

where L is the length of the pore which could be approximated to the thickness of the membrane, d and D are the small and large opening diameters of the pore respectively, κ is the specific conductivity of the electrolyte (11.377 S/m for 1 M KCl at 26 °C), V is the voltage applied across the membrane and I is the measured current.

4.2.2. Preparation of Cylindrical Nanopores. A multipore PET membrane with cylindrical nanopores was prepared by symmetric track-etching technique.[63] For this purpose, the etching solution (2 M NaOH) prepared in deionized water was filled in the etching bath. The temperature of the etching bath was maintained at 50 °C with continuously stirring by circulating heated water through the double walls of the beaker. Polymer membranes fixed in a sample holder were immersed in the preheated etching solution. During the whole process, the etching solution was continuously stirred to provide a homogeneous etchant concentration in the bath. The etching process was carried out for 4 min. After etching, the membranes were taken out from the solution and rinsed several times with distilled water. For further

removal of the residual salts, the etched membranes were additionally immersed in deionized water overnight.

4.3. Synthesis of 1-Amino-5-(2,2′:6′,2″-terpyrid-4′-yl-oxy-)pentane (terPy−DEG-NH_2). The synthesis of terPy−DEG-NH_2 ligand was carried out by following the reported method.[66] To synthesis this compound, 1.6 mg (in excess) of ground KOH flakes was added to a three-neck round-bottomed flask, and dispersed in anhydrous DMSO at 60 °C for 15 min, followed by the addition of diethylene glycolamine (DEG-NH_2, 1 mM) to the reaction chamber. The reaction was allowed to proceed for 30 min before the addition of 4′-chloro,2,2′:6′,2″-terpyridine (1 mM) into the reaction chamber. The reaction was carried out at 70 °C for 6 h. When the reaction was completed, the flask was allowed to cool down to room temperature. Then 120 mL of Millipore water was added in the flask. The reaction mixture was extracted in dichloromethane (3 × 30 mL). The organic fraction was collected and dried in anhydrous sodium sulfate, followed by evaporating the solvent in a rotary evaporator. The crude product was purified by column chromatography (DCM: methanol, 9:1). The purified compound was further characterized by ^{1}H NMR and FD-MS techniques.

^{1}H NMR (400 MHz, DMSO-d_6): 2.7 (t, 2H, CH_2, H_d), 3.2 (s, broad, NH_2), 3.5 (t, 2H, CH2, H_c), 3.82 (t, 2H, CH2, H_b), 4.35 (t, 2H, CH_2, H_a), 7.5 (ddd, 2H, CH_{terpy}, $H_{5,\ 5''}$), 7.98 (s, 2H, CH_{terpy}, $H_{3',\ 5'}$), 8.00 (m, 2H, CH_{terpy}, $H_{4,4''}$), 8.62 (d, 2H, CH_{terpy}, $H_{3,\ 3''}$), 8.72 (dd, 2H, CH_{terpy}, $H_{6,\ 6''}$) (Supporting Information Figure S1). FD-MS: [M + H] = 337 g/mol (Supporting Information Figure S2)

4.4. Functionalization of terPy−DEG-NH_2. The functionalization of terpyridine ligand on the inner walls of the nanopore was achieved by the following way. The carboxyl groups of the pore walls were first converted into an amine reactive sulfo-NHS-esters by immersing the track-etched membranes in a solution containing a mixture of *N*-(3-dimethylaminopropyl)-*N*′-ethylcarbodiimide hydrochloride (EDC, 10 mM) and *N*-hydroxysulfosuccinimide (sulfo-NHS, 20 mM) dissolved in 0.1 M MES buffer 2-(*N*-morpholino)ethanesulfonic acid, pH = 5.5. The activation of carboxyl groups was carried out for 50 min at room temperature. After the activation step, the foil was washed with the same buffer. Subsequently, the activated membranes were exposed to 10 mM solution of terPy−DEG-NH_2 prepared in the same buffer. In this step, the amine-reactive sulfo-NHS-esters were allowed to covalently couple with the terminus amine of the ligand in a reaction carried out overnight. Finally, the modified pore was washed thoroughly with buffer followed by deionized water. The same procedure was used for the modification of multinanopore membrane.

4.5. Formation of Iron−Terpyridine complexes. A solution of ferrous sulfate (100 μM) was prepared in 50% aqueous ethanol (C_2H_5OH/H_2O, 1:1 by volume). Polymer membranes (single/multipore) modified with terpyridine amine (metal chelating ligand) were exposed to a solution of ferrous sulfate for 60 min at room temperature. Subsequently, the membranes were washed first with ethanol followed by deionized water.

4.6. *I*−*V* Measurements. As-prepared (carboxylated) and ligand modified (iron−terPy complexed) single pore-membranes were mounted between the two halves of the conductivity cell. Both halves of the cell were filled with an aqueous 0.1 M KCl solution prepared in phosphate buffer (10 mM) with pH = 7.0. An Ag/AgCl electrode was placed into each half-cell solution, and a picoammeter/voltage source (Keithley 6487, Keithley Instruments, Cleveland, OH) was used to apply the desired transmembrane potential, and measure the ionic current across the single pore membrane. In the case of conical nanopores, the ground electrode was placed at the side of the membrane with the big opening of the pore. In order to record the *I*−*V* curves, a scanning triangle voltage signal from −1 to +1 V was used. The small opening of the conical nanopores was determined through the *I*−*V* recording in 1 M KCl solution.

Various concentrations of lactoferrin (LFN) protein are prepared in the same electrolyte solution, used for the measurement of respective *I*−*V* curve.

4.7. Mass-Transport Experiments. The selective diffusion of doubly charged organic analytes: methyl viologen (MV^{2+}) and 1,5-naphthalenedisulfonate (NDS^{2-}) through polymer membranes were performed before and after modification with iron−terPy ligand on the pore surface. The analyte solutions were prepared in phosphate buffer (pH 7.0). For the transport experiments, membranes were mounted between the two halves of the conductivity cell. Each cell volume was 3.4 mL with an effective permeation area of the membrane of 1.15 cm^2. The feed half-cell contained a known concentration of 10 mM of each organic analyte in the buffer solution, whereas the permeate half-cell was filled with pure buffer solution. Both solutions were continuously stirred during the whole process. Similarly, transport experiments were performed through the membranes bearing terPy−Fe(II) complex on the inner walls of the nanopores. For this purpose, lactoferrin (100 nM) was dissolved in 10 mM solution of each MV^{2+} and NDS^{2-}, respectively. After fixed time periods, the concentration of respective analyte in the permeate half-cell was determined by measuring the UV absorbance with a UNICAM UV/vis spectrometer.

■ ASSOCIATED CONTENT

Ⓢ Supporting Information. ^{1}H NMR and FD-MS spectra of 1-amino-5-(2,2′:6′,2″-terpyrid-4′-yl-oxy) pentane. This information is available free of charge via the Internet at http://pubs.acs.org/.

■ AUTHOR INFORMATION

Corresponding Author
m.ali@gsi.de, m.ali@ca.tu-darmstadt.de.

■ ACKNOWLEDGMENT

M.A., S.N., Q.H.N., and W.E. gratefully acknowledge financial support by the Beilstein-Institut, Frankfurt/Main, Germany, within the research collaboration NanoBiC. M.N.T. and W.T. are thankful to the Deutsche Forschungsgemeinschaft, the Bundesministerium für Bildung und Forschung, Germany [Center of Excellence BIOTECmarin], the European Society for Marine Biotechnology for their financial support. The authors thank Dr. Christina Trautmann from GSI (Department of materials research) for support with the heavy ion irradiation experiments.

■ REFERENCES

(1) Ali, M.; Neumann, R.; Ensinger, W. *ACS Nano* **2010**, *4*, 7267–7274.
(2) Ali, M.; Schiedt, B.; Neumann, R.; Ensinger, W. *Macromol. Biosci.* **2010**, *10*, 28–32.
(3) Ali, M.; Yameen, B.; Neumann, R.; Ensinger, W.; Knoll, W.; Azzaroni, O. *J. Am. Chem. Soc.* **2008**, *130*, 16351–16357.
(4) Fologea, D.; Gershow, M.; Ledden, B.; McNabb, D. S.; Golovchenko, J. A.; Li, J. L. *Nano Lett.* **2005**, *5*, 1905–1909.
(5) Iqbal, S. M.; Akin, D.; Bashir, R. *Nat. Nanotechnol.* **2007**, *2*, 243–248.
(6) Mara, A.; Siwy, Z.; Trautmann, C.; Wan, J.; Kamme, F. *Nano Lett.* **2004**, *4*, 497–501.
(7) Storm, A. J.; Storm, C.; Chen, J. H.; Zandbergen, H.; Joanny, J. F.; Dekker, C. *Nano Lett.* **2005**, *5*, 1193–1197.
(8) Vlassiouk, I.; Kozel, T. R.; Siwy, Z. S. *J. Am. Chem. Soc.* **2009**, *131*, 8211–8220.

(9) Jirage, K. B.; Hulteen, J. C.; Martin, C. R. *Science* **1997**, *278*, 655–658.
(10) Kohli, P.; Harrell, C. C.; Cao, Z. H.; Gasparac, R.; Tan, W. H.; Martin, C. R. *Science* **2004**, *305*, 984–986.
(11) Martin, C. R.; Nishizawa, M.; Jirage, K.; Kang, M. S.; Lee, S. B. *Adv. Mater.* **2001**, *13*, 1351–1362.
(12) Nishizawa, M.; Menon, V. P.; Martin, C. R. *Science* **1995**, *268*, 700–702.
(13) Savariar, E. N.; Krishnamoorthy, K.; Thayumanavan, S. *Nat. Nanotechnol.* **2008**, *3*, 112–117.
(14) Bruehwiler, D.; Ritter, H.; Ramm, J. H.; Dieu, L. Q.; Bauer, C.; Dolamic, I.; Gartmann, N. *Chimia* **2009**, *63*, 8–13.
(15) Sinha, P. M.; Valco, G.; Sharma, S.; Liu, X. W.; Ferrari, M. *Nanotechnology* **2004**, *15*, S585–S589.
(16) Spohr, R.; Reber, N.; Wolf, A.; Alder, G. M.; Ang, V.; Bashford, C. L.; Pasternak, C. A.; Omichi, H.; Yoshida, M. *J. Controlled Release* **1998**, *50*, 1–11.
(17) Hille, B. *Ionic Channels of Excitable Membranes*; 3rd ed.; Sinauer Associates Inc.: Sunderland, MA, 2001.
(18) Dekker, C. *Nat. Nanotechnol.* **2007**, *2*, 209–215.
(19) Healy, K.; Schiedt, B.; Morrison, A. P. *Nanomedicine* **2007**, *2*, 875–897.
(20) Hou, X.; Guo, W.; Jiang, L. *Chem. Soc. Rev.* **2011**, *40*, 2385–2401.
(21) Howorka, S.; Siwy, Z. *Chem. Soc. Rev.* **2009**, *38*, 2360–2384.
(22) Siwy, Z. S.; Howorka, S. *Chem. Soc. Rev.* **2010**, *39*, 1115–1132.
(23) Spohr, R. *Radiat. Meas.* **2005**, *40*, 191–202.
(24) Trautmann, C. In *Ion Beams in Nanoscience and Technology*; Hellborg, R., Whitlow, H., Zhang, Y., Eds.; Springer: New York, 2009.
(25) Korchev, Y. E.; Bashford, C. L.; Alder, G. M.; Apel, P. Y.; Edmonds, D. T.; Lev, A. A.; Nandi, K.; Zima, A. V.; Pasternak, C. A. *FASEB J.* **1997**, *11*, 600–608.
(26) Siwy, Z.; Apel, P.; Dobrev, D.; Neumann, R.; Spohr, R.; Trautmann, C.; Voss, K. *Nucl. Instrum. Methods Phys. Res., Sect. B* **2003**, *208*, 143–148.
(27) Siwy, Z.; Fulinski, A. *Phys. Rev. Lett.* **2002**, *89*, 198103.
(28) Siwy, Z. S. *Adv. Funct. Mater.* **2006**, *16*, 735–746.
(29) Wolf, A.; Siwy, Z.; Korchev, Y. E.; Reber, N.; Spohr, R. *Cell. Mol. Biol. Lett.* **1999**, *4*, 553–565.
(30) Apel, P. Y.; Korchev, Y. E.; Siwy, Z.; Spohr, R.; Yoshida, M. *Nucl. Instrum. Methods Phys. Res., Sect. B* **2001**, *184*, 337–346.
(31) Siwy, Z.; Heins, E.; Harrell, C. C.; Kohli, P.; Martin, C. R. *J. Am. Chem. Soc.* **2004**, *126*, 10850–10851.
(32) Ali, M.; Ramirez, P.; Mafe, S.; Neumann, R.; Ensinger, W. *ACS Nano* **2009**, *3*, 603–608.
(33) Ali, M.; Schiedt, B.; Healy, K.; Neumann, R.; Ensinger, W. *Nanotechnology* **2008**, *19*, 085713.
(34) Gyurcsanyi, R. E. *TrAC, Trends Anal. Chem.* **2008**, *27*, 627–639.
(35) Hou, X.; Jiang, L. *ACS Nano* **2009**, *3*, 3339–3342.
(36) Umehara, S.; Karhanek, M.; Davis, R. W.; Pourmand, N. *Proc. Nat. Acad. Sci. U.S.A.* **2009**, *106*, 4611–4616.
(37) Wang, J.; Martin, C. R. *Nanomedicine* **2008**, *3*, 13–20.
(38) Siwy, Z.; Trofin, L.; Kohli, P.; Baker, L. A.; Trautmann, C.; Martin, C. R. *J. Am. Chem. Soc.* **2005**, *127*, 5000–5001.
(39) Ali, M.; Bayer, V.; Schiedt, B.; Neumann, R.; Ensinger, W. *Nanotechnology* **2008**, *19*, 485711.
(40) Siwy, Z.; Dobrev, D.; Neumann, R.; Trautmann, C.; Voss, K. *Appl. Phys.* **2003**, *76*, 781–785.
(41) Ali, M.; Mafe, S.; Ramirez, P.; Neumann, R.; Ensinger, W. *Langmuir* **2009**, *25*, 11993–11997.
(42) Ali, M.; Tahir, M. N.; Siwy, Z.; Neumann, R.; Tremel, W.; Ensinger, W. *Anal. Chem.* **2011**, *83*, 1673–1680.
(43) Hou, X.; Guo, W.; Xia, F.; Nie, F. Q.; Dong, H.; Tian, Y.; Wen, L. P.; Wang, L.; Cao, L. X.; Yang, Y.; Xue, J. M.; Song, Y. L.; Wang, Y. G.; Liu, D. S.; Jiang, L. *J. Am. Chem. Soc.* **2009**, *131*, 7800–7805.
(44) Xia, F.; Guo, W.; Mao, Y. D.; Hou, X.; Xue, J. M.; Xia, H. W.; Wang, L.; Song, Y. L.; Ji, H.; Qi, O. Y.; Wang, Y. G.; Jiang, L. *J. Am. Chem. Soc.* **2008**, *130*, 8345–8350.
(45) Ali, M.; Yameen, B.; Cervera, J.; Ramirez, P.; Neumann, R.; Ensinger, W.; Knoll, W.; Azzaroni, O. *J. Am. Chem. Soc.* **2010**, *132*, 8338–8348.
(46) Ali, M.; Ramirez, P.; Tahir, M. N.; Mafe, S.; Siwy, Z.; Neumann, R.; Tremel, W.; Ensinger, W. *Nanoscale* **2011**, *3*, 1894–1903.
(47) Sexton, L. T.; Horne, L. P.; Sherrill, S. A.; Bishop, G. W.; Baker, L. A.; Martin, C. R. *J. Am. Chem. Soc.* **2007**, *129*, 13144–13152.
(48) Jagerszki, G.; Gyurcsanyi, R. E.; Hofler, L.; Pretsch, E. *Nano Lett.* **2007**, *7*, 1609–1612.
(49) Holyer, R. H.; Hubbard, C. D.; Kettle, S. F. A.; Wilkins, R. G. *Inorg. Chem.* **1966**, *5*, 622–625.
(50) Tuccitto, N.; Giamblanco, N.; Licciardello, A.; Marletta, G. *Chem. Commun.* **2007**, 2621–2623.
(51) Tuccitto, N.; Giamblanco, N.; Marletta, G.; Licciardello, A. *Appl. Surf. Sci.* **2008**, *255*, 1075–1078.
(52) Baker, E. N.; Baker, H. M. *Cell. Mol. Life Sci.* **2005**, *62*, 2531–2539.
(53) Baker, H. M.; Baker, E. N. *Biometals* **2004**, *17*, 209–216.
(54) Qiu, J. Z.; Hendrixson, D. R.; Baker, E. N.; Murphy, T. F.; Geme, J. W., St; Plaut, A. G. *Proc. Nat. Acad. Sci. U.S.A.* **1998**, *95*, 12641–12646.
(55) Baker, E. N.; Anderson, B. F.; Baker, H. M.; MacGillivray, R. T. A.; Moore, S. A.; Peterson, N. A.; Shewry, S. C.; Tweedie, J. W. *Adv. Exp. Med. Biol.* **1998**, *443*, 1−14.
(56) Moore, S. A.; Anderson, B. F.; Groom, C. R.; Haridas, M.; Baker, E. N. *J. Mol. Biol.* **1997**, *274*, 222–236.
(57) Ji, B.; Maeda, A.; Higuchi, M.; Inoue, K.; Akita, H.; Harashima, H.; Suhara, T. *Life Sci.* **2006**, *78*, 851–855.
(58) Hu, K. L.; Li, J. W.; Shen, Y. H.; Lu, W.; Gao, X. L.; Zhang, Q. Z.; Jiang, X. G. *J. Controlled Release* **2009**, *134*, 55–61.
(59) Marchetti, M.; Pisani, S.; Antonini, G.; Valenti, P.; Seganti, L.; Orsi, N. *Biometals* **1998**, *11*, 89–94.
(60) Orsi, N. *Biometals* **2004**, *17*, 189–196.
(61) Valenti, P.; Antonini, G. *Cell. Mol. Life Sci.* **2005**, *62*, 2576–2587.
(62) Jenssen, H.; Hancock, R. E. W. *Biochimie* **2009**, *91*, 19–29.
(63) Nguyen, Q. H.; Ali, M.; Bayer, V.; Neumann, R.; Ensinger, W. *Nanotechnology* **2010**, *21*, 365701.
(64) Yameen, B.; Ali, M.; Neumann, R.; Ensinger, W.; Knoll, W.; Azzaroni, O. *Nano Lett.* **2009**, *9*, 2788–2793.
(65) Wolf-Reber, A. Aufbau eines Rasterionenleitwertmikroskops. Stromfluktuationen in Nanoporen, PhD Dissertation, Johann Wolfgang Goethe Universität, Frankfurt am Main, Germany, 2002.
(66) Sahoo, J. K.; Tahir, M. N.; Yella, A.; Branscheid, R.; Kolb, U.; Tremel, W. *Langmuir* **2011**, *27*, 385–391.
(67) Hermanson, G. T. *Bioconjugate Techniques*; Academic Press: San Diego, CA, 1996.
(68) Karnik, R.; Duan, C. H.; Castelino, K.; Daiguji, H.; Majumdar, A. *Nano Lett.* **2007**, *7*, 547–551.
(69) Umehara, S.; Pourmand, N.; Webb, C. D.; Davis, R. W.; Yasuda, K.; Karhanek, M. *Nano Lett.* **2006**, *6*, 2486–2492.
(70) Wei, C.; Bard, A. J.; Feldberg, S. W. *Anal. Chem.* **1997**, *69*, 4627–4633.
(71) White, H. S.; Bund, A. *Langmuir* **2008**, *24*, 2212–2218.
(72) Cervera, J.; Schiedt, B.; Neumann, R.; Mafe, S.; Ramirez, P. *J. Chem. Phys.* **2006**, *124*, 104706.
(73) Ramirez, P.; Apel, P. Y.; Cervera, J.; Mafe, S. *Nanotechnology* **2008**, *19*, 315707.
(74) Constantin, D.; Siwy, Z. S. *Phys. Rev. E* **2007**, *76*, 041202.
(75) Kosinska, I. D.; Goychuk, I.; Kostur, M.; Schmid, G.; Hänggi, P. *Phys. Rev. E* **2008**, *77*, 031131.
(76) Stein, D.; Kruithof, M.; Dekker, C. *Phys. Rev. Lett.* **2004**, *93*, 035901.
(77) Lee, S. B.; Martin, C. R. *Anal. Chem.* **2001**, *73*, 768–775.